Advection Diffusion Model for Particle Assisted Solar Water Evaporation

Sai Kiran Hota, Gerardo Diaz

School of Engineering, University of California – Merced, Merced 95343 CA (USA)

Abstract

Particle assisted solar water evaporation is attracting attention in the area of low temperature desalination as well as heating and power generation. Activated carbon (AC1) is one such material that can lend to efficient evaporation process for water desalination. A coupled heat and mass transfer model with volumetric heat exchange accounting for convective mass exchange at higher temperatures is presented. Here an advection-diffusion (Ad-Di) evaporation model is adopted to predict the evaporation rate of water with nanoparticle-assisted heating. A volume fraction of 0.1% is considered to account for high heat localization. The nanoparticle is assumed to be spherical at a uniform size of 80nm. Temperature of the fluid-particle system rises, and the Ad-Di model is used to predict the evaporation rate. The employed high mass transfer model showed that the warmer fluid evaporates faster but is affected by the ambient heat losses. Higher ambient temperatures (50°C for a 50°C fluid) results in a longer evaporation time than the ambient at 40°C.

keywords: Advection-diffusion (Ad-Di) model, Mie theory, Volumetric heating.

1. Introduction

Traditional clean water production has high dependence on energy from fossil fuels. Combating the environmental impact, solar driven vapor generation for clean water production has garnered widespread attention. This approach is sustainable with little to no carbon footprint. Taylor et al., (Taylor, et al., 2012) were among the first investigators to describe the possibility of steam generation in a nanofluid. Since then, numerous steam generation techniques have been discussed involving nanofluids and floating structures. These employ efficient photo-thermal conversion materials such as plasmons (Chen, et al., 2018) or carbon-based materials (Wang, et al., 2017). Likewise, composites and nature derived products have been proposed as efficient and alternative means for vapor and steam generation (Liu, et al., 2017; Wilson, et al., 2019; Zhu, et al., 2019).

Owing to surface plasmon resonance effects, plasmon based materials convert light into heat. These materials are usually characterized by sharp peaks for absorption and reflectance spectrum. Neumann et al., (Neumann, et al., 2013) discussed steam generation from nanofluids exposed to focused solar light. They employed gold nanoparticles in their study as a means of high-temperature steam generation for medical sterilization. Effects of varying sizes and shapes of gold nanoparticles on steam generation was also identified (Guo, et al., 2017 pp. 4815-4824; Zhou, et al., 2017 pp. 195-200). In addition to gold, possibility of using copper (Lin, et al., 2019), silicon (Ishii, et al., 2016), silver (Wang, et al., 2017) and core-shell composites (Li, et al., 2017) were investigated.

Carbon based nanofluids, on the other hand, have been found to be highly efficient vapor / steam generation systems. They are characterized by broader absorption along the solar spectrum and are more economical than the expensive plasmons (Zeiny, et al., 2018). Different forms of carbon based nanofluids such as carbon black, carbon nanotubes, graphene and graphene oxide have been investigated (Ni, et al., 2015; Wang, et al., 2016; Ghafurian, et al., 2019). Li et al (Li, et al., 2018) have demonstrated the superiority in using activated carbon fiber felt for steam generation.

doi:10.18086/swc.2019.46.02 Available at http://proceedings.ises.org

The process of vapor generation involves volumetric heating in the fluid and evaporation from the open surface. While Fick's diffusion process is enough to describe the evaporation at lower temperature, at higher temperatures, convective (advection) mass transfer is also needed to be accounted for. In this article, the evaporation process involving the advection-diffusion model with volumetric heating from nanoparticles under solar light will be investigated.

2. Theoretical approach

The fluid-particle dispersion interacts with the incoming sunlight where the absorbed light intensity is converted into heat. This contributes to volumetric heating of the fluid. The fluid system exchanges both energy and mass at the open surface. The typical heat and mass transfer equations follow the energy balance (F. Mills, 2001)

I. Top surface: $\dot{m}"h_{fg_{nf}} = K_{nf}\frac{dT}{dY} + h(T_\infty - T) + \epsilon\sigma(T_\infty^4 - T^4) + Q$ (eq.1)

II. Inner layer: $(\rho C_p)_{nf}\frac{dT}{dt} = K_{nf}\frac{dT}{dt} + Q$ (eq.2)

The above equations represent the energy balance for heat and mass transfer. The left-hand term in the first equation indicates the evaporating flux and is the mass transfer term. The last term in the right-hand side is the volumetric heating by absorption. The following subsections will describe the above terms in detail.

2.1 Volumetric heat generation (**Q**)

The volumetric heat generated by the absorbing nanoparticle is computed by calculating the extinction coefficient. Mie theory (for size $k_pX \approx 1$) is employed in computing extinction coefficient by firstly calculating scattering and absorption efficiency by solving for Mie coefficients a_n and b_n (Modest, 2013). As shown in Fig. 1(a) and 1 (b), Mie theory is known to converge with commonly used Rayleigh theory for nanoparticles and geometric optics for larger particles (Sai Kiran Hota, 2018; Modest, 2013).

Scattering efficiency and absorption efficiency are calculated as

$Q_{sca} = \frac{2}{X^2}\sum_{n=1}^{\infty}(2n+1)(|a_n|^2 + |b_n|^2)$ (eq.3)

$Q_{abs} = \frac{2}{X^2}\sum_{n=1}^{\infty}(2n+1)\,\Re\{a_n + b_n\}$ (eq.4)

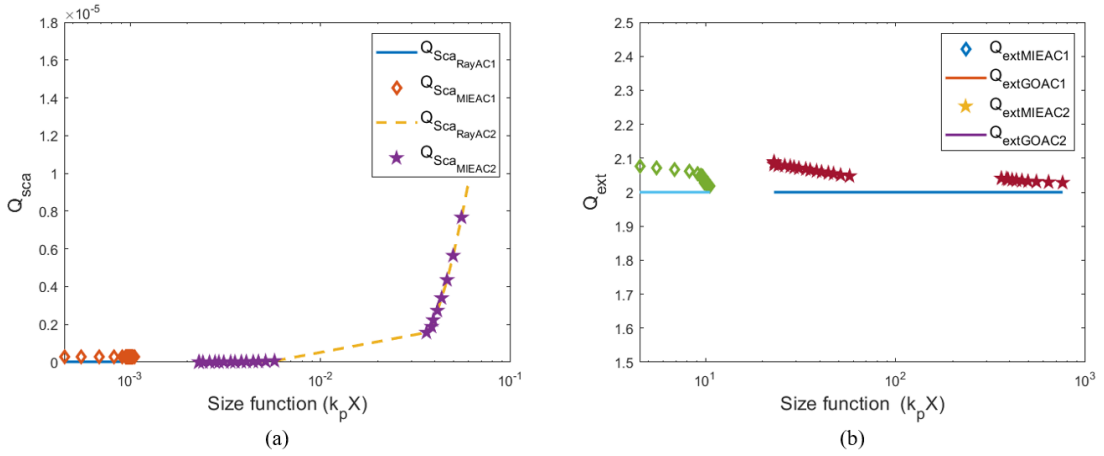

Figure 1 Convergence of Mie solution with (a) Rayleigh theory (Ray) and (b) geometric optics (GO) for activated carbon (AC1) and amorphous carbon (AC2)

As the size increases, it is seen from Figure 1(a) and 1(b) that the Mie theory converges with Rayleigh and

geometric optics. The absorption and scattering efficiency lend to the calculation of extinction efficiency as the summation of absorption and scattering efficiency.

$$Q_{ext} = Q_{abs} + Q_{sca} \quad \text{(eq.5)}$$

Considering uniform sized particles and attenuation in the base fluid, extinction coefficient of the fluid-particle system is given as:

$$\beta_{ext} = 1.5\frac{f_v}{d_p} Q_{ext} + (1 - f_v)\frac{4\pi k_f}{\lambda} \quad \text{(eq.6)}$$

where k_f is the attenuation coefficient of the base fluid.

Light attenuates as it traverses the fluid-particle system. This drop-in intensity can be given as a function of extinction coefficient by the simplified form of Beer-Lambert law given as:

$$\frac{dI}{dy} = -\beta_{ext} y \quad \text{(eq.7)}$$

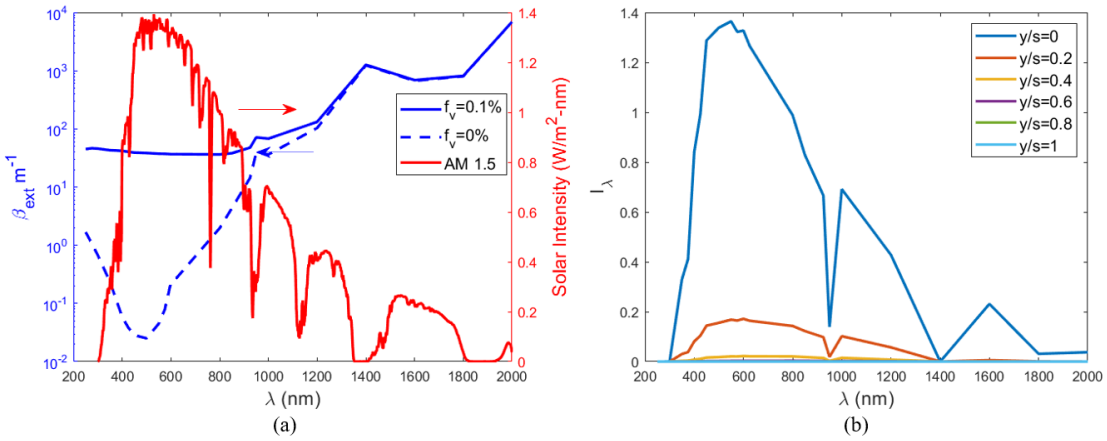

Figure 2: (a) Extinction coefficient of the nano fluid system; (b) Intensity attenuation of solar intensity for a total path length of 10mm

Figure 2 (a) shows the extinction coefficient of 0.1% volume activated carbon dispersion against pure water. This stark superiority helps in high solar absorptivity and hence excellent photo-thermal conversion. At 0.1% volume fraction, almost all light is attenuated within the path length of only 10 mm. The corresponding intensity attenuation along the depth of the light travel is shown in Fig. 2(b).

The fraction of solar absorptivity potential along the path length can be calculated by the weighted solar absorption coefficient (A_{sol}) calculated as:

$$A_{sol} = \frac{\int_{\lambda_{min}}^{\lambda_{max}} (1 - \exp(-\beta_{ext} y) d\lambda}{\int_{\lambda_{min}}^{\lambda_{max}} I_\lambda d\lambda} \quad \text{(eq.8)}$$

The Figures 3 (a) and 3(b) show that the light attenuates a little over 10mm of path travel. The available radiative heat which contributes to volumetric heating is available in that portion only. It can be deduced that little to no heat will be available at layers below 10mm length. However, any reduction in volume fraction will lead to reduced attenuation and thereby increased path length travel. This will lead to overall increase in bulk liquid temperature rather than localized heating. Hence, 0.1% of volume fraction is chosen in this study for subsequent analysis.

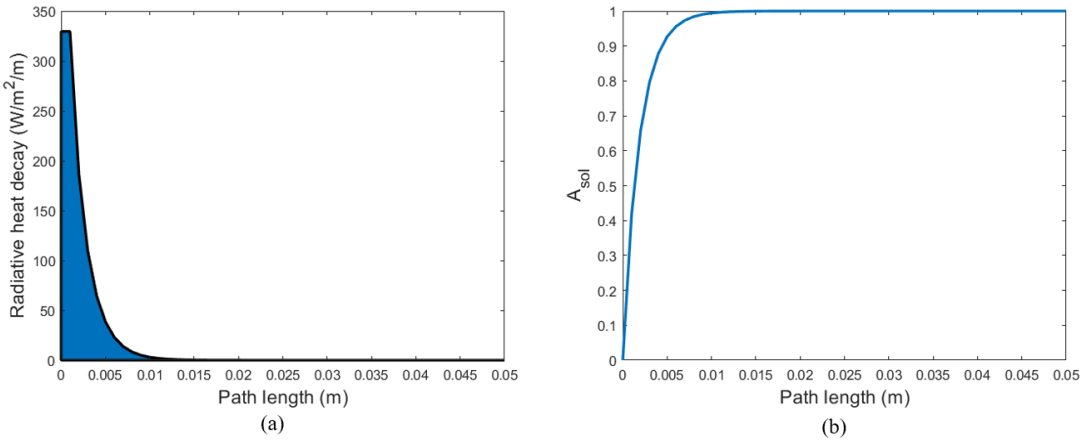

Figure 3: (a) radiative decay due to intensity attenuation; (b) weighted solar absoroption coefficient along path length

2.2 Energy exchange

The radiative heat loss term is included in the governing equations 1 and 2. The open surface loses sensible heat from top (F. Mills, 2001). The sensible heat loss can be described as a convection process where the heat transfer coefficient depends on average air properties and Nusselt number. The set of applied empirical coefficients and their applicable limits are tabulated below in Table.1

Table 1Parameters for sensible heat loss

Parameter	**Empirical terms**
Convection coefficient (h)	$h_{sensible} = Nu\frac{k_f}{\delta}$
Nusselt number (Nu) (Pauken, 1999)	$Nu = \left(Nu_{free}^{n} + Nu_{forced}^{n}\right)^{\frac{1}{n}}; \quad n = 2$
Nusselt number (free)	$Nu_{free} = \begin{cases} 0.54\,(GrPr)^{\left(\frac{1}{4}\right)}; if\ GrPr < 2 * 10^{7}\ \ (Laminar\ free) \\ 0.14(GrPr)^{\frac{1}{3}}; Otherwise\ (Turbulent\ free) \end{cases}$
Nusselt number (forced)	$Nu_{forced} = \begin{cases} 0.332\,(Re^{\frac{1}{2}}Pr^{\frac{1}{3}}); if\ RePr < 3 * 10^{5}\ \ (Laminar\ forced) \\ 0.0336\left(Re^{0.8}Pr^{\frac{1}{3}}\right); Otherwise\ (Turbulent\ forced) \end{cases}$

In addition to sensible heat loss, radiative heat loss should also be taken into consideration. Radiative heat transfer coefficient is a subset of radiative heat flux computations and is calculated as

$$h_{radiative} = \epsilon\sigma(T^2 + T_\infty^2)(T + T_\infty) \qquad \text{(eq.9)}$$

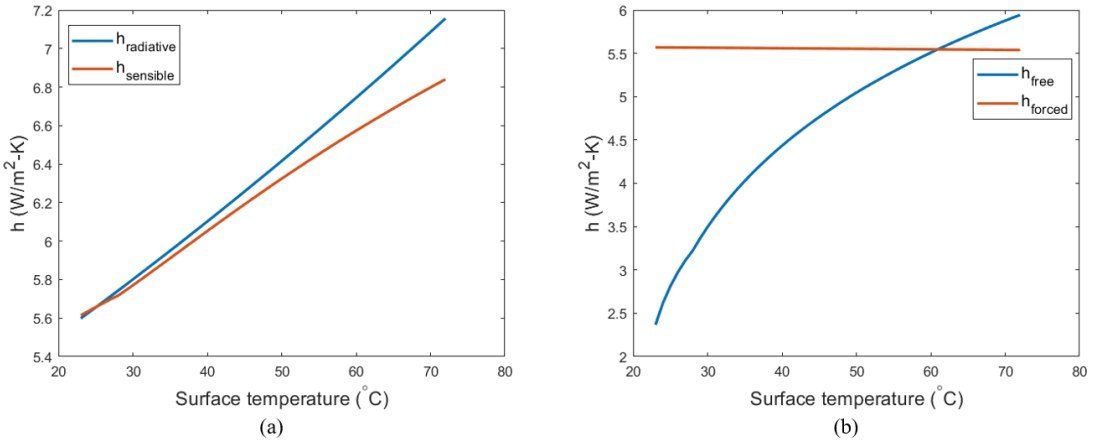

Figure 4: (a) contribution of sensible (convective) and radiative heat transfer coefficients; (b)respective contributions of free and forced convective coefficient at moderate ambient velocity of 2m/s

Figure 4(a) shows the contribution of radiative and convective heat transfer coefficient. For water emissivity of 0.96 (Brewster, 2018) and a moderate ambient velocity of 2 m/s, the respective heat transfer coefficients are comparable to each other. It is known that a forced convection condition increases the evaporation rate (Ohri, et al., 2019).

2.3 Mass transfer analysis

The open surface evaporates simultaneously while exchanging energy with surroundings. The evaporation occurs as vapor diffusion due to mass fraction gradient. At lower temperatures, the evaporation process follows Fick's law of diffusion ($m_{1,s} - m_{1,e} < 0.1$). At higher volume fractions, as the surface temperature increases, Fick's law of diffusion underpredicts due to the increase in vapor mass fraction. Convective mass flux at this point is no longer negligible. Hence, high mass transfer rate theory (F. Mills, 2001) must be adopted. This is an advection diffusion (Ad-Di) model accounting for transfer of one species into the other (Botham, 2015), e.g., water vapor into air. The differential form of mass flux, (Steeman, et al., 2009) is given as

$$\dot{m}" = -\frac{\rho D_{v,a}}{1-m_1}\frac{dm_1}{dy}\Big|_{y=o} \quad \text{(eq.3)}$$

Upon derivation and simplification, the evaporating mass flux rate can be given as

$$\dot{m}" = g_{m1} B_{m1} \quad \text{(eq.4)}$$

where g_{m1} is the mass conductance and B_{m1} is the blowing parameter given as:

$$B_{m1} = \frac{m_{1,e}-m_{1,s}}{m_{1,s}-1} \quad \text{(eq.5)}$$

The evaporation mass flux, to fit all contexts of diffusion and advection transfer is collectively given as

$$\dot{m}" = g^*_{m1} \log\frac{(1+B_{m1})}{B_{m1}}\, B_{m1} \quad \text{(eq.6)}$$

where g^*_{m1} is the zero-mass transfer limit conductance and $\log\frac{(1+B_{m1})}{B_{m1}}$ is the driving force.

At low mass transfer rates, where $m_{1,s}$ is very small, $B_{m1} \to 0$. In such cases, the advection term is ignored and

$$\lim_{B_{m1}\to 0} \log\frac{(1+B_{m1})}{B_{m1}} = 1 \quad \text{(eq.7)}$$

Which leads to a modified form of (eq.3) as denoted by Fick's law of diffusion (Diff) as

$$\dot{m}" = -\rho D_{v,air} \frac{dm_1}{dy} \quad \text{(eq.8)}$$

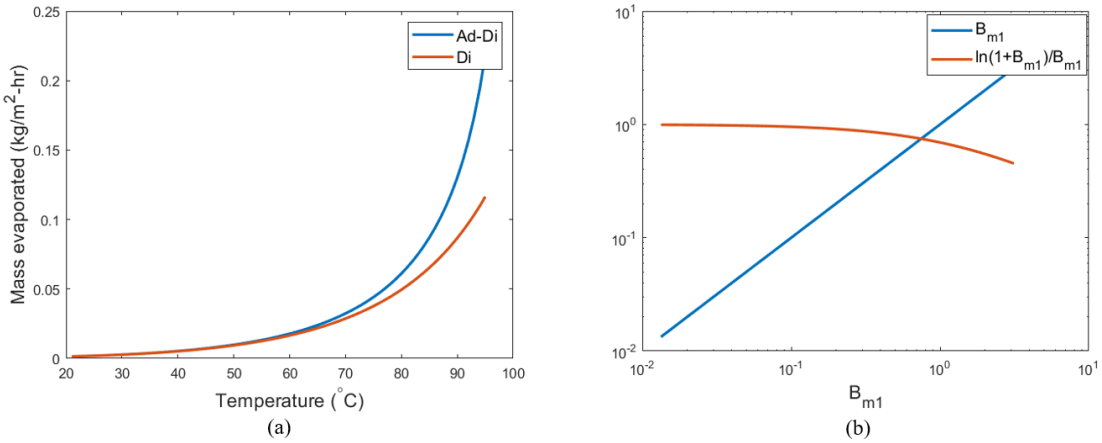

Figure 5: (a) Fick's law of Diffusion against Advection-Diffusion (Ad-Di) model (b) Deviation of Ad-Di model from Diff model

Figure 5(b) shows that, at low temperatures (<50°C), the blowing force is much less than 1 and as a result, the driving force approaches unity. The advection term vanishes at this point and the evaporation rate predicted by the Ad-Di model approaches the Diff model as is seen in Fig. 5(a).

3. Problem description

Nanofluid (fluid-particle) dispersion system is considered akin to a simple solar still except for an open surface for interaction with surrounding. This set up is similar to experiments performed by (Ishii, et al., 2016; Wang, et al., 2016) and many others. Here we consider a unit surface with 10cm deep container as described in (Hota, et al., 2019). The ambient is at a constant temperature of 50°C and a relative humidity of 50%, to emulate high temperature conditions (eg., coastal India). Time taken for evaporation of 0.03 kg (≈30 ml) of water from the container is computed. The dispersion system interacts with solar spectrum with airmass (AM) 1.5 as depicted in Fig.1 (a), where the assumptions involved are

- Nanoparticles are spherical and uniform size with no substantial size distribution. The size of the nanoparticle is 80 nm.
- The incident solar spectrum doesn't attenuate before interacting with the open surface.
- Walls are insulated and the bottom surface is purely reflecting.
- The dispersion is uniformly distributed through the length of the container.

The thermo-physical properties of nanofluids are given as (M. Shaker., et al., 2014; Pak, et al., 1998):

$$\frac{K_{nf}}{K_f} = \frac{2K_f + K_p + 2f_v(K_p - K_f)}{2K_f + K_p - f_v(K_p - K_f)} \quad \text{(eq.9)}$$

$$C_{p_{nf}} = f_v C_{p_p} + (1 - f_v) C_{p_f} \quad \text{(eq.10)}$$

$$\rho_{nf} = f_v \rho_p + (1 - f_v) \rho_f \quad \text{(eq.11)}$$

The coupled heat and mass transfer equations are solved simultaneously in a transient manner. Volume fraction and the system temperature are continuously tracked and updated at each step. The updated temperature field leads to calculating the contribution of system heat losses through sensible and radiative loss at the surface, conduction heat through the dispersion system. However, in this system, volume fraction of 0.1% attains a full intensity absorption within the top 10% of path travel, thereby relatively the bottom layers are at lower temperature and heat is distributed only in the top. Another contribution for this heat localization comes from the fact that the thermal conductivity of the fluid-particle dispersion is close to water which is only ≈ 0.6 W/m-K. Hence, considerable temperature difference between the top and the bottom layers is maintained due to the structuring of the overall energy transfer.

4. Evaporation rate: high mass transfer rate model (Ad-Di) model

As the fluid evaporates, the nanoparticle concentration increases with time, thereby the temperature of the fluid increases. Hence, with time, the convective mass flux also becomes important and must be considered. The following figure compares the evaporation rate of the water between Di model and Ad-Di model.

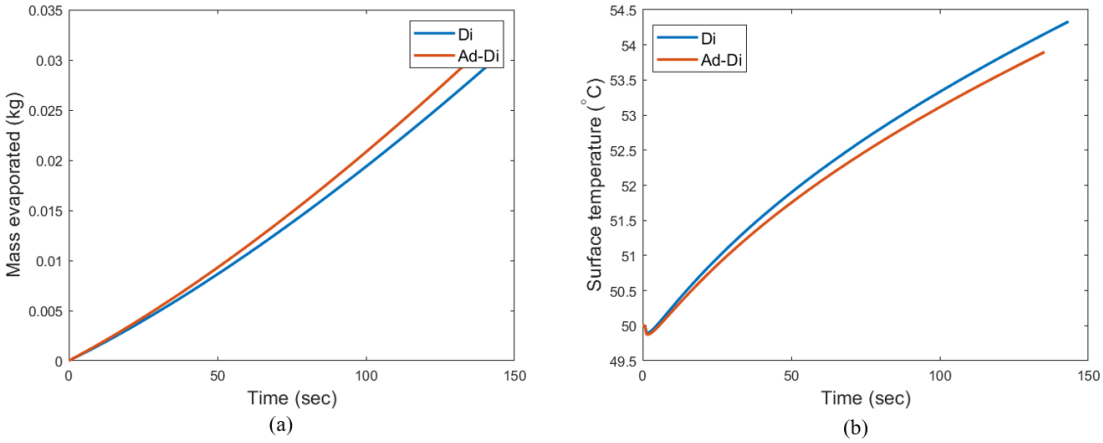

Figure 6 Comparison between diffusion (Di) only and High mass transfer rate (Ad-Di) model. (a) Mass evaporated against time; (b) Surface temperature

Figures 6 (a) and 6 (b) show the differences in prediction of evaporation rate between low mass transfer (Di) only model and high mass transfer (Ad-Di) model along with the evolution of surface temperature at 50℃. While the surface temperature shows proximity to each other, the trend shows that, as the evaporation continue, a larger difference will be obtained with Di model underpredicting the evaporation rate.

5. Temperature distribution and surface temperature

As water evaporates, along with volume fraction, the surface temperature also increases simultaneously. The increasing volume fraction leads to further localization of heat as the attenuation length is reduced.

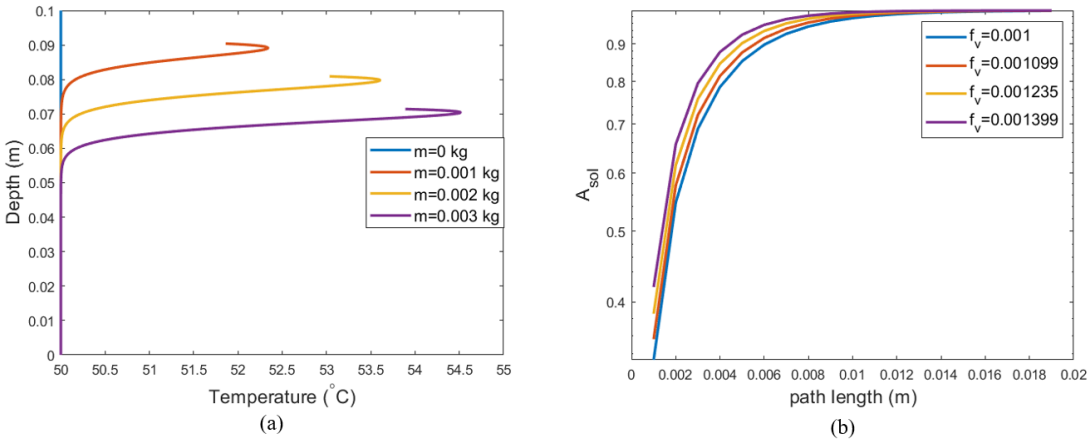

Figure 7: (a)Temperature distribution and corresponding (b) solar light attenautaion at available volume fraction

Figure7 (a) shows the temperature distribution along the depth of the fluid-particle system. As time increases, the surface temperature increases, and the depth is reduced indicating that water is evaporating. The temperature profile is shown after water evaporation of 0 kg, 0.001 kg, 0.002 kg and 0.003 kg. The dip near the open surface indicates that the open surface is also losing heat to the surroundings through convection and radiation. The effective heat localization can be seen to have heated the fluid only in the top layer showing higher temperature than the collective bulk volume. The Fig.7 (b) shows the respective A_{sol} for different f_V at

the corresponding instances. The light attenuation and path travel decrease with increasing volume fraction.

6. Evaporation and transient variation of temperature and volume fraction

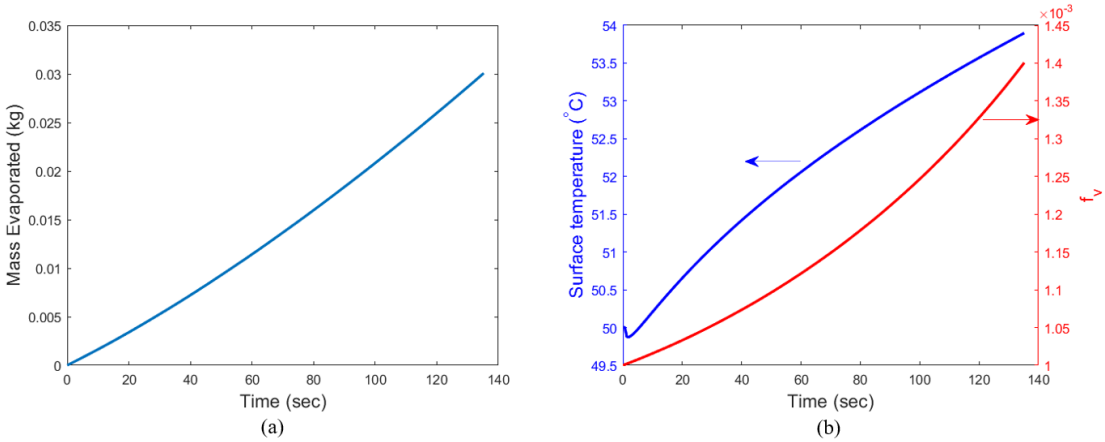

Figure 8: (a) Rate of mass evaporation; (b) Transient change in surface temperature and volume fraction

Figure 8(a) shows the evaporation rate of water with time. Under the given conditions, the time required for evaporation of 0.03 kg of water was found to be just a over 2 min (135 s). Consecutively, as the water evaporates, the surface temperature was found to increase continuously as seen in Fig. 8(b). This can be explained by the transient increase in volume fraction which increases the heat localization at the top surface (show in Fig. 7 (b)) while keeping the bulk volume cool.

7. Predicted evaporation rate under different ambient conditions

Evaporation rate drastically varies with temperature. It is known that warmer fluid evaporates faster due to higher vapor mass fraction (Hota, et al., 2019). At lower temperature, with low mass fraction, the advection term of mass transfer is very low and Ad-Di model is in semblance with the Di model, as shown in Fig. 5 (a). As the temperature increases, the mass evaporation rate increases. However, it is non-linear due to the variables involved as well as transient effects resulting in heat losses.

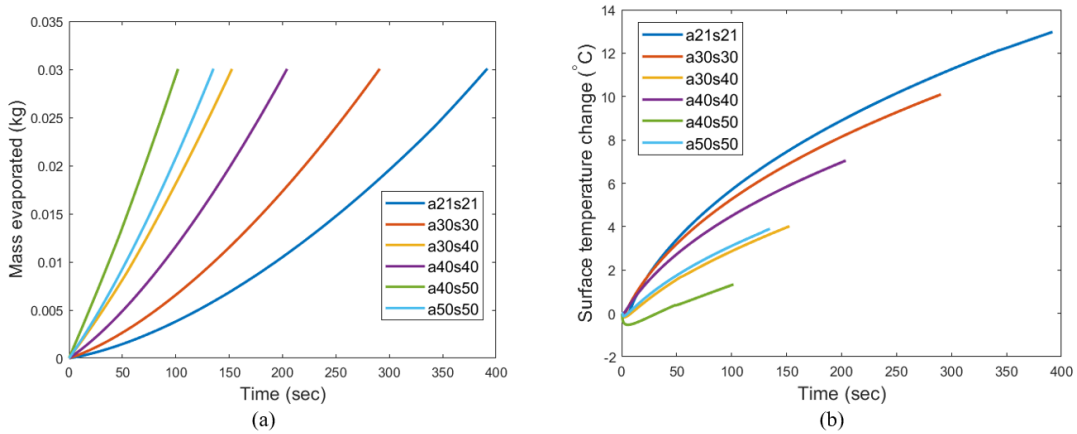

Figure 9: (a) Predicted evaporation rate; (b) Change in surface temperature, at different conditions. a: indicates ambient and s: surface initial conditions

Figure 9 (a) shows the mass evaporation rate of water along with the corresponding change in surface temperature. At low initial conditions, as is expected, water takes longer to evaporate, while the surface

temperature rise is found to be more than 13.5°C. The time taken for evaporation was found to be 390 s. As the temperature increases, the evaporation curve almost becomes linear. The temperature change in the surface follows a mixed pattern due to differences in contribution of evaporation heat exchange and the cooling effects (heat losses). At 40°C for the system and ambient temperature, the temperature rise and evaporation time were 7°C and 204 s. While the vaporization time almost reduces by half to 102 s at 40°C ambient and 50°C system temperature, the temperature change is only 1.3°C. Interestingly, the surface temperature change and vaporization time, as seen in Fig. 9 (b) increase to 135s and 3.9°C respectively when the system and ambient are at 50°C. At this point, it can be understood that the heat loss coefficients are higher than the other condition thereby leading to reduction in evaporation rate.

8. Conclusion

Published theoretical investigations consider only Diffusion (Di) based model for evaporation of water. However, at higher temperatures this model underpredicts mass transfer since the process also depends on the convective term. Here, we consider the Ad-Di model accounting for both diffusion and advection process for mass exchange in the coupled heat and mass transfer model for a fluid containing nanoparticles.

At low temperatures, with driving force approaching unity (Fig. 5), the Ad-Di model converges with Di model. Also, along with the Mie theory, we take advantage of both Rayleigh theory and geometric optics for faster computation as opposed to only Mie theory for fluid-particle and light interaction. This is justified as Mie theory converges with both Rayleigh theory for very small particles and geometric optics (Fig. 1).

As water evaporates, the volume fraction continuously increased and as a result more heat was localized. The surface temperature was also found to increase as a result. The surface temperature increase was found to be highest at lower temperature conditions of 21°C. The surface temperature increased by more than 13.5°C while the time taken for evaporation of 0.03 kg of water was almost 400 s while at warmer conditions, time required for water evaporation reduced. At 40°C ambient and 50°C fluid (system) initial temperatures, the evaporation rate was found to be the highest with water evaporating within 102 s. Further increasing the ambient temperature to 50°C, the evaporation rate dropped a little to 135 sec while the surface temperature increased from 1.3°C to 3.9°C.

In all the cases, heat generation was well localized near the surface. This can be attributed to the high extinction coefficient of the system leading to efficient light trapping within 10 mm of light travel. The light penetration decreased as the transient volume fraction increased due to evaporation, leading to more efficient heat localization. The observed small dip in surface temperature in Fig. 7 is due to simultaneous cooling effect (heat loss) from the surface. Through the above results, we propose activated carbon as another source of carbon that shows promise as an efficient vapor generation fluid system.

9. Acknowledgements

The authors acknowledge the support of the California Energy Commission #GFO-16-503. The help extended by UC Solar and constructive comments by Dr. Michael Modest is appreciated.

Nomenclature

A_{sol}	Weighted solar absorption coefficient	
a_n, b_n	Mie coefficients	
C_p	Specific heat capacity	(J/Kg-k)
$D_{v,a}$	Mass diffusivity	(m^2/s)
f_v	Volume fraction	
h	Heat transfer coefficient	(W/m^2-k)
h_{fg}	Enthalpy of vaporization	(J/kg)
I	Incident light intensity	(W/m^2-nm)
K	Thermal conductivity	(W/m-k)
k	Attenuation coefficient	
$\dot{m}$"	Mass flux	(kg/m^2-s)
$m_{1,s}, m_{1,e}$	Mass fractions (vapor and air)	
Q	Heat flux	(W/m^2)
$Q_{abs,\ sca,\ ext}$	Absorption/ scatterin/ extinction effiicency	
T	Temperature	(°C)
X	Size parameter $X = \frac{2\pi n_f}{\lambda} r_p$; n_f: fluid refractive index	
y	Path length	(m)
Greek Letters		
β_{ext}	Extinction coefficient	(m^{-1})
ϵ	emissivity	
∞	Ambient	
ρ	density	(kg/m^3)
σ	Stefan Boltzmann constant	($5.67X10^{-8}$ W/m^2-k^4)
Subscripts		
p	particle	
f	fluid	
nf	nanofluid/ fluid-particle system	

10. References

Aimen Zeiny [et al.] Solar evaporation via nanofluids: A comparative study [Journal].-[s.1.]: Renewable Energy, 2018. -Vol. 122. -pp. 443-454

Ankang Guo [et al.] Diameter effect of gold nanoparticles on photothermal conversion for solar steam generation [Journal]. - [s.l.] : The Royal Society of Chemistry, 2017. - Vol. 7. -pp. 4815-4824

Anthony F.Mills Mass Transfer [Book]. - [s.l.] : Pretince Hall Inc., 2001.

Bock Choon Pak and Young I. Cho HYDRODYNAMIC AND HEAT TRANSFER STUDY OF DISPERSED FLUIDS WITH SUBMICRON METALLIC OXIDE PARTICLES [Journal]. - [s.l.] : Experimental Heat Transfer, 1998. - 2 : Vol. 11. -pp. 151-170

Chuanlu Chen [et al.] Dual functional assymetric plasmonic structures for solar water purification and pollution detection [Journal]. - [s.l.] : Nano Energy, 2018. - Vol. 51. -pp. 451-456

George Ni [et al.] Volumetric solar heating of nanofluids for direct vapor generation [Journal]. - [s.l.] : Nano Energy, 2015. - Vol. 17. -pp. 290-301

George Sidebotham Heat Transfer Modelling An Inductive Approach [Book]. - [s.l.] : Springer International, 2015.

H. J. Steeman [et al.] Evaluation of different definitions of the convective mass transfer coefficient for water evaporation into air [Journal]. - [s.l.] : International Journal of Heat and Mass Transfer, 2009.-15-16: Vol. 52. -pp: 3757-3766

Hailong Wang, Lei Miao and Sakae Tanemura Morphology Control of Ag Polyhedron Nanoparticles for Cost-Effective and Fast Solar Steam Generation [Journal]. - [s.l.] : Solar RRL , 2017. - Vol. 1. -pp. 1600023

Haoran Li [et al.] Commercially Available Activated Carbon Fiber Felt enables Efficient Solar Steam Generation [Journal]. - [s.l.] : ACS Applied Materials & Interfaces, 2018. - 11 : Vol. 10. -pp. 9362-9368

Haoran Li [et al.] Synchronous steam generation and heat collection in a broadband Ag@TiO2 core-shell nanoparticle-based receiver [Journal]. - [s.l.] : Applied Thermal Engineering, 2017. - Vol. 121. -pp. 617-627

Higgins M. Wilson [et al.] Ultra-low cost cotton based solar evaporation device for seawater desalination and waste water purification to produce drinkable water [Journal]. - [s.l.] : Desalination, 2019. - Vol. 456. -pp. 85-96

Lin Zhou [et al.] Self-assembled spectrum selective plasmonic absorbers with tunable bandwidth for solar energy conversion [Journal]. - [s.l.] : Nano Energy, 2017. - Vol. 32. -pp. 195-200

Liu Huidong [et al.] A bioinspired capillary-driven pump for solar vapor generation [Journal]. - [s.l.] : Nano Energy, 2017. - Vol. 42. -pp. 115-121

M. Quinn Brewster Evaporation of water at high mass-transfer rates by natural convection air flow with application to spent-fuel pools [Journal]. - [s.l.] : International Journal of Heat and Mass Transfer, 2018. - Vol. 116. -pp. 703-714

M. Shaker, E. Birgersson and A.S. Majumdar Extended Maxwell model for the thermal conductivity of nanofluids that accounts for nonlocal heat transfer [Journal]. - [s.l.] : International Journal of Thermal Sciences, 2014. - Vol. 84. -pp. 260-266

Mengmeng Zhu [et al.] Carbonized Daikon for high efficient solar steam generation [Journal]. - [s.l.] : Solar Energy Materials and Solar Cells, 2019. - Vol. 191. -pp. 83-90

Michael F. Modest Radiative Heat Transfer [Book]. - [s.l.] : Elsevier, 2013.

Michael T. Pauken An experimental investigation of combined turbulent free and forced evaporation [Journal]. - [s.l.] : Experimental Thermal and Fluid Science, 1999. - Vol. 18. -pp. 334-340

Mohammad Mustafa Ghafurian [et al.] Localized solar heating via graphene oxide nanofluid for solar steam generation [Journal]. - [s.l.] : Journal of Thermal Analysis and Calorimetry, 2019. - Vol. 135. -pp. 1443-1449

Oara Neumann [et al.] Compact solar autoclave based on steam generation using broadband light-harvesting nanoparticles [Journal]. - [s.l.] : PNAS, 2013. - 29 : Vol. 110. -pp. 11677-11681

Robert A. Taylor [et al.] Characterization of light-induced, volumetric steam generation in nanofluids [Journal]. - [s.l.] : International Journal of Thermal Sciences, 2012. - Vol. 56. -pp. 1-11

Sai Kiran Hota and Gerardo Diaz Particle size effects of solar absorbing dispersions in water and convergence of Mie solutions // UC Solar Symposium. - San Francisco : UC Solar, 2018.

Sai Kiran Hota and Gerardo Diaz Activated carbon dispersion as absorber for solar water evaporation: A parametric analysis [Journal]. - [s.l.] : Solar Energy, 2019. - Vol. 184. -pp. 40-51

Satoshi Ishii [et al.] Solar water heating and vaporization with silicon nanoarticles at mie resonances [Journal]. - [s.l.] : Optical Materials Express, 2016. - 2 : Vol. 6. -pp. 642-648

Virender Ohri and Vikrant Khullar Using Solar Energy for Water Purification Through Nanoparticles Assisted Evaporation [Journal]. - [s.l.] : Journal of Solar Energy Engineering, 2019. -1: Vol. 141. -pp. 011008

Xinzhi Wang [et al.] Direct vapor generation through localized solar heating via carbon-nanotube nanofluid [Journal]. - [s.l.] : Energy Conversion and Management, 2016. - Vol. 130. -pp. 176-183

Xinzhi Wang [et al.] Enhanced direct steam generation via a bio-inspired solar heating method using carbon nanotube films [Journal]. - [s.l.] : Powder Technology, 2017. - Vol. 321. -pp. 276-285

Yawen Lin [et al.] Copper nanoparticles with near-unity, omnidirectional, and broadband optical absorption for highly efficient solar steam generation [Journal]. - [s.l.] : IOP Nanotechnology, 2019. - Vol. 30. -pp. 015042

Yuchao Wang, Lianbin Zhang and Peng Wang Self-Floating Carbon Nanotube Membrane on Macroporous Silica Substrate for Highly Efficient Solar-Driven Interfacial Water Evaporation [Journal] // ACS Sustainable Chemistry & Engineering. - 2016. - pp. 1223-1230.